



# Crystallite Size Dependence on Structural Parameters and Photocatalytic Activity of Microemulsion Mediated Synthesized ZnO Nanoparticles Annealed at Different Temperatures

By J. Sharma, M. Vashishtha & D. O. Shah

*Dharmsinh Desai University, India*

**Abstract-** The synthesis of ZnO nanoparticles has attracted considerable interest because of their unique properties and potential applications in a variety of solid state devices, catalytic media etc. By using water-in-oil (w/o) microemulsions, nanodroplets of water were used as chemical reactor to synthesize nanoparticles of zinc oxide. Addition of reducing agent ( $(\text{NH}_4)_2\text{CO}_3$ ) and zinc salt ( $\text{Zn}(\text{NO}_3)_2$ ) followed by heat treatment results in the formation of zinc oxide nanoparticles (NPs). The structural and optical properties of the samples were investigated by X-ray diffraction and UV-VIS-NIR absorption spectroscopy. X-ray diffraction revealed the wurtzite structure of ZnO. Percentage of lattice contraction and average particle size of the sample were also calculated from the XRD. Size-dependent blue shifts of absorption spectra revealed the quantum confinement effect. Furthermore, on increasing annealing temperature of ZnO NPs, crystallite size increases which, in turn, decreases the band gap energy and photocatalytic degradation efficiency of phenol.

**Keywords:** *microemulsion, ZnO nanoparticles, size-selective catalysis.*

**GJSFR-B Classification :** *FOR Code: 259999p*



*Strictly as per the compliance and regulations of :*



RESEARCH | DIVERSITY | ETHICS

# Crystallite Size Dependence on Structural Parameters and Photocatalytic Activity of Microemulsion Mediated Synthesized ZnO Nanoparticles Annealed at Different Temperatures

J. Sharma<sup>α</sup>, M. Vashishtha<sup>σ</sup> & D. O. Shah<sup>ρ</sup>

**Abstract-** The synthesis of ZnO nanoparticles has attracted considerable interest because of their unique properties and potential applications in a variety of solid state devices, catalytic media etc. By using water-in-oil (w/o) microemulsions, nanodroplets of water were used as chemical reactor to synthesize nanoparticles of zinc oxide. Addition of reducing agent ((NH<sub>4</sub>)<sub>2</sub>CO<sub>3</sub>) and zinc salt (Zn(NO<sub>3</sub>)<sub>2</sub>) followed by heat treatment results in the formation of zinc oxide nanoparticles (NPs). The structural and optical properties of the samples were investigated by X-ray diffraction and UV-VIS-NIR absorption spectroscopy. X-ray diffraction revealed the wurtzite structure of ZnO. Percentage of lattice contraction and average particle size of the sample were also calculated from the XRD. Size-dependent blue shifts of absorption spectra revealed the quantum confinement effect. Furthermore, on increasing annealing temperature of ZnO NPs, crystallite size increases which, in turn, decreases the band gap energy and photocatalytic degradation efficiency of phenol.

**Keywords:** microemulsion, ZnO nanoparticles, size-selective catalysis.

## 1. INTRODUCTION

Controlling the size and shape of many metal oxides particles is essential in many advanced applications [1-2]. ZnO, which is a wide band gap semiconductor material with a direct band gap of 3.37eV, is an exceptionally important material for wide applications in areas such as photo catalysis, semiconductors and UV detectors [1-2]. It absorbs ultraviolet (UV) light through a process of electronic excitation between the valence band and conduction band. In conjunction with its high chemical stability and low toxicity, this property of ZnO renders it suitable for

use as a UV-screening agent in a diverse range of applications.

Due to its suitable band gap, high thermal stability, non-toxicity, photoactivity and of reasonably low cost, ZnO has been a preferred material for photocatalytic applications. In this respect, it has been utilized traditionally not only to produce useful chemicals [3], but also to convert pollutants in waste streams in innocuous or less harm form [4-6].

ZnO nanomaterials have been synthesized using various methods, including vapor-phase transport [7], chemical vapor deposition [8], magnetron sputtering [9], laser ablation [10], and wet chemical methods [11]. It is conceived that wet chemical routes provide a promising option for the large-scale production of various ZnO nanoparticles. However, these wet chemical methods often face the problem of shape and size control of the products [11].

Compared with the simple solution route, the reverse microemulsion approach, has a special advantage in the synthesis of nanoparticles. Reverse microemulsion is a thermodynamically stable phase separation of water-in-oil aided by a surfactant, where the surfactant shells and water-droplet cores constitute micelles with radii ranging from 5 to 100 nm. The synthesis reaction is confined in the nanodroplets of water, thus the size and shape of the products could be tailored by varying the droplet diameter, whereas the surfactant film can inhibit the aggregation of nanodroplets [11-14].

In this communication, we have attempted to use the microemulsion method for synthesis of ZnO nanoparticles. In this method, initially, small water droplets with a narrow size distribution are formed in a hydrophobic solvent. Then, the reaction takes place in the water droplet, generating zinc oxide nanoparticles with a narrow size distribution. In this paper, we report the effect of annealing temperatures on crystallite size, band gap energy and photocatalytic activity of ZnO nanoparticles.

**Author α σ:** Department of Chemical Engineering & Shah-Schulman Center for Surface Science and Nanotechnology, Faculty of Technology, Dharmsinh Desai University, College Road, Nadiad, Gujarat, India. e-mail: shjyoti\_06@yahoo.com

**Author ρ:** Department of Chemical Engineering & Shah-Schulman Center for Surface Science and Nanotechnology, Faculty of Technology, Dharmsinh Desai University, College Road, Nadiad, Gujarat, India, Department of Chemical Engineering and Anesthesiology, University of Florida, Gainesville, FL, USA.

## II. EXPERIMENTAL

### a) Materials and Methods

All the chemical (analytical grade reagents) were purchased from Merck Chemical Reagent Co. Ltd. and used without further purification. To prepare the microemulsion n-octane, CTAB and Pentanol were mixed in weight ratio 5:3:2 by magnetically stirring until the mixture became transparent. The two microemulsion solution containing different reactants were prepared as follows: The microemulsion (ME-1) containing  $Zn(NO_3)_2$  reactant was obtained by adding 6 ml of a 0.5M  $Zn(NO_3)_2$  aqueous solution to 20ml of oil+ CTAB +Pentanol mixture. Similarly, the microemulsion (ME-2) containing  $(NH_4)_2CO_3$  reactant was prepared by adding 5.6 ml of a 0.5M  $(NH_4)_2CO_3$  aqueous solution to 20ml oil +CTAB+ Pentanol mixture.

The mixing was done by continuous stirring. ME-1 was added dropwise to the ME-2 under stirring. The mixture of ME-1 and ME-2 was stirred for 6 hours at room temperature. The precipitates was collected by centrifugation at 5000 rpm and washed separately with water and ethanol several times prior to drying in a oven at 80°C until a constant weight was achieved. Finally, the precursor was annealed at different temperatures (400°C to 600°C) for 1 hour. Figure 1 shows the flow chart for the synthesis procedure of ZnO NPs.

### b) Characterization

The prepared ZnO nanoparticles were characterized for their phase identification and optical properties. X-ray diffraction pattern for the ZnO NPs was recorded using X-ray diffractometer (Bruker, Advanced D8) with Cu  $K_\alpha$  radiation ( $\lambda = 1.5418 \text{ \AA}$ ) and Lynx Eye detector to study the crystalline nature, type of phase and the crystallite size in the sample. The sample was scanned in  $2\theta$  range of  $0^\circ - 90^\circ$  with a scanning rate of  $0.02^\circ \text{ s}^{-1}$ . Crystallite size of each sample (D nm) was determined from the peak of maximum intensity (101) of the phase using Scherrer formula with a shape factor ( $\beta$ ) of 0.9 using the XRD line broadening method [15-21]:

$$D = 0.89\lambda/\beta \cos \theta \quad (1)$$

Where 0.89 is Scherrer's constant,  $\lambda$  is the wavelength of X-rays,  $\theta$  is the Bragg diffraction angle, and  $\beta$  is the full width at half-maximum (FWHM) of the diffraction peak corresponding to plane and D is the diameter (nm) of a crystallite. The corrected peak breadth was determined by subtracting out the instrumental contribution to the peak breadth from the measured peak width [22].

The inter planar spacing (d) and lattice parameter was evaluated using the relations (2) and (3) :

$$2d \sin\theta = n \lambda \quad (2)$$

$$1/d^2 = 4/3 (h^2+hk+k^2) /a^2 + l^2/c^2 \quad (3)$$

Here,  $\theta$  is the angle of diffraction,  $\lambda$  is the wavelength of x ray, (hkl) are the Miller indices and a, c are the lattice parameters.

The % Interplaner shift in the sample was evaluated using the relation (4):

$$\% \text{ Interplaner shift} = [(\text{standard } d - \text{observed } d) / \text{standard } d] \times 100 \quad (4)$$

The diameter of nanodroplets in microemulsion used in making ZnO NPs was measured by dynamic light scattering using Malvern particle size analyzer and is shown in figure 2. The diameter comes out to be 10.66 nm. These nanodroplets might afford a confined environment for the growth of nanoparticles in the nanometer region. The thermogravimetric analysis was carried out using Mettler Toledo TGA/DTA thermal analyser. The analysis was protected by nitrogen and carried out at a temperature range of 20- 800°C and at a heating rate of 10°C/min.

Morphology of the sample was investigated using scanning electron microscope (SEM with ZEISS). Samples were formed using a suspension of ZnO particles dispersed in distilled water by ultrasonic treatment. A few drops of dilute dispersion were deposited onto a carbon film taped to an aluminium grid and dried in air. The optical transmission/absorption spectra of ZnO were recorded using a UV-VIS-NIR spectrophotometer (Agilent, Carry 5000) in the wavelength range 200- 800 nm.

### c) Photocatalytic Activity

Synthesized ZnO NPs were utilized for the photocatalytic degradation of phenol under UV light. In this experiment, phenol was premixed with distilled water to obtain 30 ppm concentration and the study of its photocatalytic degradation was carried out after continuous stirring. Before the degradation processes, 5 ml of 30 ppm phenol solution was mixed with 0.005g of ZnO materials calcined at different temperatures to obtain required solutions of catalyst loading with 1000 ppm concentration. These samples were then allowed to be irradiated under UV light for a fixed time duration in order to observe the effect of ZnO calcined at different temperatures on the degradation processes of Phenol.

After the UV light irradiation for a certain time interval, each sample was centrifuged to separate the suspensions of the ZnO nanoparticles. The concentration of Phenol was measured by UV-VIS-NIR spectrophotometer using Carry 5000 detector with a scan rate of 120 nm /min in the range of 200 nm to 800 nm. The rate of degradation was studied in terms of changes of the absorption maximum at the absorption peak of 269.75 nm. The photo degradation efficiency of phenol was calculated applying the following equation:

$$\% \text{ Photo degradation efficiency} = C_0 - C / C_0 \times 100 \quad (5)$$

Where  $C_0$  (in ppm) is the initial phenol concentration ; C (in ppm) is the retained phenol in solution.

### III. RESULTS AND DISCUSSIONS

#### a) Phase Analysis (X-ray diffraction)

X-ray diffraction is a non-destructive and analytical method for identification and quantitative analysis of various crystalline forms of prepared nanoparticles also known as phases present in the samples. The XRD patterns of ZnO nanoparticles calcined at temperatures 400°C, 450°C, 500°C, 550°C and 600°C for 1 hour are shown in figure 3(a)-3(e) respectively. These patterns were recorded by using Bruker D8 Advance diffractometer employing Cu-K $\alpha$  radiations in the 2 $\theta$  range 10°- 80°. A definite line broadening of the XRD peaks indicates that the prepared material consist of particles in nanoscale range. From this XRD patterns analysis, we determined peak intensity, position and full-width at half-maximum (FWHM) data.

All strong diffraction peaks are located at (100), (002), (101), (102), (110), (103) and (112) which have been clearly indexed as hexagonal wurtzite phase (JPCDS card number: 05-0664) of ZnO with lattice constants  $a = 0.324$  nm and  $c = 0.520$  nm. The diffraction peaks are sharper with the increase of the annealing temperature, which implies that the crystalline structure tends to more integrity and also the average particle size grows up with increasing annealing temperature as shown in figure 4 and the results are given in Table 1.

From Table 1, It has been observed that change in annealing temperature causes change in crystallize size. This may be due to the fact that, in ZnO nanoparticles, there are a large no of vacancies of oxygen, vacancy clusters, and local lattice disorders present at the interface, which leads to the decrease in the volume of the unit cell. The low temperature annealing can lead to a relaxation in the interface structure, but cannot dispel the local lattice disorders or change the internal structure of the nanograins, so there are no apparent changes in the positions and intensities of XRD peaks. When the annealing temperature increases there is a rapid decrease in the density of vacant lattice sites, vacancy clusters and local lattice disorders and a rapid resumption of lattice parameters and the volume of the unit cell towards normal values, and the grains begin to grow. Hence the particle size increases with increasing annealing temperature [23]. The average particle size, crystallinity and % interplaner shift at different annealing temperature are also tabulated in Table.1

The origin of Lattice contraction is due to the presence of dangling bonds in the surface layer of ZnO nanoparticles. The ions on the surface of ZnO nanoparticles are incompletely coordinated and possess the unpaired electron orbitals. Each of these dangling bonds (Zn<sup>2+</sup> and O<sup>2-</sup> ions) forms an electric dipole resulting in a parallel array of dipoles originating

in the boundary layer of each nanoparticles lies in this surface and experience a repulsive force. ZnO has the property of adsorbing O<sup>2-</sup> and O<sup>-</sup> ions in the surface; hence the repulsive interdipolar force decreases and the attractive electrostatic interaction between Zn<sup>2+</sup> and O<sup>2-</sup> increases. Due to this electrostatic attraction, lattice is slightly contracted. The change in % lattice error with calcination temperature is shown in figure 5.

#### b) SEM Analysis

The SEM is used to produce high-resolution imaging of shapes of substances and to confirm spatial variations in chemical compositions. Figure 6 represents the SEM pictures of ZnO nanoparticles at different annealing temperatures. These pictures confirm the formation of ZnO nanoparticles. These pictures substantiate the approximate spherical shape to the nanoparticles. The SEM of all four samples clearly rectifies the effect of sintering temperature on its surface morphology. The amount of porosity as well as size of pores decreases as sintering temperature is increased. Also the surface gets modified and become smoother for higher annealing temperature. The morphology of nanoparticles reveals that they form nanoclusters at higher temperatures [24-26] i.e. average grain size increased with annealing temperature. This is consistent with XRD results.

#### c) Band Gap Analysis (UV-VIS-NIR Absorption Spectrum)

The size of the nanoparticles plays an important role in changing the entire properties of materials. Thus, size evolution of semiconducting, nanoparticles becomes very essential to explore the properties of the materials. UV-visible absorption spectroscopy is widely being used technique to examine the optical properties of nanosized particles. Figure 7 shows the UV-visible absorption spectra of ZnO nanoparticles after annealing at different temperatures. The band gap energy was calculated on the basis of maximum absorption spectrum of ZnO nanoparticles according to equation:

$$E_g = 1240 / \lambda \quad (6)$$

Where  $E_g$  is the band gap energy and  $\lambda$  is the lower cut off wavelength (nm) of the nanoparticles [27].

A UV spectrum provides information about optical band gap of the material. The energy band of the material is related to the absorption coefficient  $\alpha$  by the Tauc relation (7):

$$\alpha h\nu = A (h\nu - E_g)^n \quad (7)$$

Where A is constant,  $\alpha$  is the optical absorption coefficient,  $h\nu$  is photon energy,  $E_g$  is band gap and  $n = 1/2$  for allowed direct transition. It is clear that the absorption edge shifts to the lower wavelength or higher energy with decreasing size of the nanoparticles. This shift in the absorption edge is due to the quantum size effect. As the annealing temperature increase, the peak

absorption wavelength become red shifted due to decreasing quantum confinement with increasing particle size as shown in figure 8 and the results are given in Table 2.

ZnO nanoparticles did not show clear band gap absorption due to the strong light scattering caused by the large particle size. This might be also due to the aggregation of the particles at higher calcinations temperatures [27-30]

#### d) Effect of nanocrystallite size on Photocatalytic Activity

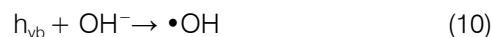
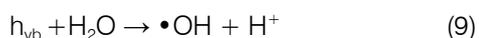
The UV-vis absorption spectra for photodegradation of phenol using ZnO are presented in figure 9. As can be seen, the photocatalytic efficiency of ZnO decreases with increasing calcination temperature. Decreasing the average particle size increases the number of surface sites available for charge transfer. However, decreasing the particle size also increases the rate of surface charge recombination. For a sufficiently small particle size, surface recombination becomes the dominant process as the charge carriers are formed close to the particle surface and also because the recombination process is faster than interfacial charge transfer [31].

As the annealing temperature increases, photocatalytic degradation of phenol by ZnO NPs decreases due to the formation of larger particle size at higher temperature, thereby reduces the surface area and no. of active sites on the photocatalyst surface, which in turn decrease the no. of Hydroxyl and superoxide radicals. Thus lower degree of degradation [31-34] (Figure 10 &11).

Mechanism of photodegradation of phenol can be explained as follows. When the photocatalyst ZnO is irradiated with ultraviolet (UV) radiation from sunlight or other illuminated light source (e.g. fluorescent lamps), it produces electron–holes pairs on or near the surface (Eq. (8)) through electron transfer from the valence band to the conduction band across the band gap of the semiconductor. This state is referred as the semiconductor's photo-excitation state. The electron–hole pair quickly diffuses to the surface. These photogenerated electron–hole pairs can recombine within a time scale of nanoseconds to radiate heat. Such a short lifetime would not allow the electrons and holes to participate in any chemical reaction.



Therefore, the electrons and holes should be captured by any of chemical species which exist on the surface (ions, atoms, molecules, etc.), or by the so-called surface traps. Hydroxyl radicals are generated when the surface adsorbed water or hydroxyl anions react with the valence band hole of the UV excited ZnO (Eqs 9-10).



Superoxide radicals are generated by the interaction of atmospheric oxygen or dissolved oxygen of the reaction solution with the conduction band electrons of the UV excited ZnO (Eq.11):



These hydroxyl and superoxide radicals attack the adsorbed phenolic compound as long as illumination is continued, or the mineralization of the phenol is completed.

## IV. CONCLUSIONS

The temperature range of 400 - 600°C was chosen for annealing the sample and to see its effect on crystallize size, band gap and photocatalytic activity. From the above experimental results, following conclusions can be made:

Results of x-ray pattern show that all peaks can be well indexed to the wurtzite phase of ZnO. It also reveal that the lattice slightly contracted due to the presence of dangling bonds on the surface layer of ZnO. In SEM micrographs, the morphology of nanoparticles reveals that they form nanoclusters at higher annealing temperatures i.e. average grain size increased with calcination temperature. This is consistent with XRD results. Absorption peak of the prepared sample is highly blue shifted as compared to the bulk (360nm). Large band gap energy and highly blue shifted absorption edge confirmed that the prepared ZnO nanoparticle exhibit strong quantum confinement effect. As the annealing temperature increases, the particle size of the sample increases. It did not show clear band gap absorption due to the strong light scattering caused by the large particle size. This might be also due to the aggregation of the particles at higher calcinations temperatures.

Photochemical results showed that crystallize size affects the photodegradation. As the particle size increases, the degradation efficiency decreases due to the reduction of the surface area and no. of active sites on the photocatalyst surface, which in turn decrease the no. of Hydroxyl and superoxide radicals.

## V. ACKNOWLEDGEMENTS

We acknowledge CSIR, New Delhi for providing financial support for the successful completion of this work. We are grateful to I.I.T. Kanpur for their kind cooperation in SEM analysis. We are thankful to Dr. Multani for giving their suggestions.

## REFERENCES RÉFÉRENCES REFERENCIAS

1. U. Ozgur, Y. I. Alivov, A. Teke, M. A. Reshchikov, S. Dogan, V. Avrutin, S. J. Cho and H. Morkoc, J. Appl. Phys.98 (2005) 041301.

2. A.B. kashyout, M. Soliman, M. EL Gamal, M. fathy, Mater. Chem. Phys.90 (2005) 230.
3. M.A. Fox, Acc. Chem. Res. 16 (1983) 314–321.
4. H. Yoneyama, Y. Yamashita, H. Tamura, Nature 282 (1979) 817–818.
5. K. Kogo, H. Yoneyama, H. Tamura, J. Phys. Chem. 84 (1980) 1705–1710.
6. A.L. Pruden, D.F. Ollis, J. Catal. 82 (1983) 404–417.
7. Wu, Y. Y.; Yang, P. D. J. Am. Chem. Soc.123 (2001) 3165.
8. Park, W. I.; Yi, G. C.; Kim, M.; Pennycook, S. J. Adv. Mater.24 (2002)1841
9. E. Pal, T. Seemann, V. Zllmer, M. Busse, D\_ek\_ any, J. Colloid Polym. Sci .287(2009) 481.
10. A. M. Morales, C.M. Liber, Science 279 (1998) 208.
11. M.P. Pileni, Nat. Mater. 2 (2003) 145.
12. M. Boutonnet, J. Kizling, P. Stenius, G. Maire, Colloids Surf. 5 (1982) 209.
13. S. Vaucher, M. Li, Angew S. Mann, Chem., Int. Ed.39 (2000) 1793.
14. C.M. Bender, J.M. Burlitch, D. Barber, C. Pollock, Chem. Mater. 12 (2000) 1969.
15. H. Hofmeister, G. L. Tan, M. Dubeil, J. Mater.20 (2005) 55.
16. C. Hammond, The Basic of Crystallography and Diffraction, Oxford University Press, NY, 1997.
17. N. Okereke, A. J. Ekpunobi, Pelagia Research Library -Advances in Applied Science Research 3 (3) (2012) 1244.
18. T.K. Patil, I.M. Talele, Pelagia Research Library-Advances in Applied Science Research, 3 (3) (2012) 1702.
19. H. Zhang, W. R. Lacefield, J. Biomater. 21 (2000) 23.
20. A. Sharma, Pallavi, S. Kumar, S. Dahiya , N. Budhiraja, *Advances in Applied Science Research* 4(1) (2013)124.
21. S. Srikantha, N. Suriyanarayananb, S. Prabahara, V. Balasubramaniana, D. Kathirvelc., Pelagia Research Library-Advances in Applied Science Research 2 (1)(2011) 95.
22. [Cullity B., 1978. Elements of X-Ray Diffraction. 2nd edn. Addison-Wesley, Reading.
23. Soosen Samuel M, Lekshmi Bose and George KC, ISSN: 0973-7464, 16 (2009) 57-65.
24. K.J.Toda, *J.Alloys Comps.* 665 (2006)408.
25. C.H. Yang, T.C. Yang, Y.K. Chic, *J Electrochem Soc* 3(2005) 152.
26. K. J. Toda, *J. Alloys Compds.*665(2006) 408.
27. Y. H. Tong, L. Dong, Y. C. Liu, D. X. Zhao, J. Y. Zhang, Y. N. Lu, D.Z. Shen, X. W. Fan, Mater. Lett. 61 (2007) 3578.
28. R. Basca, Y. Kihn, M. Verelst, J. Dexpert, W. Basca, P. Serp, Surf. Coat. Technol. (2008).
29. D. S. Kim, S. J. Han, S. Y. Kwak, J. Colloid Interface Sci. #16 (2007) 85.
30. R. J. Davis and Z. Liu, "Titania-silica: a model binary oxide catalyst system," Chemistry of Materials 9 (1997)2311–2324.
31. A.C. Dodd, A.J. McKinley, M. Saunders and T. Tsuzuki, Journal of Nanoparticle Research 8(2006) 43–51.
32. Masoud Rastegar, Alireza Zolfaghari, and Hamidreza Naderi, Proceedings of the International Conference on Nanotechnology: Fundamentals and Applications Ottawa. Ontario, Canada. Aug. (2010).
33. Kodihalli G. Chandrappa, Thimmappa V. Venkatesha, *Nano-Micro Letters* 4(1)(2012) 14-24.
34. Di Li, Hajime Haneda, *Chemosphere* 51(2003)129–137.

*Table 1 :* 2θ, % Lattice contraction, Crystallize size & % Crystallinity of (101) plane for ZnO nanoparticle at different annealing temperature

Temperature (°C)	2 Theta 2θ	Observed d	% Interplaner Shift	Crystallize Size (nm)	Crystallinity %
400	36.323	2.4704	0.19	11.18	86.23
450	36.335	2.4695	0.23	11.66	89.60
500	36.359	2.4680	0.30	14.86	91.20
550	36.444	2.4624	0.52	19.44	93.00
600	36.480	2.4601	0.61	21.28	94.52

*Table 2 :* Band gap energy, C/C<sub>0</sub> & % degradation efficiency for ZnO nanoparticles at different annealing temperatures

Crystallize Size (nm)	Band gap Energy (eV)	C/C <sub>0</sub> (For 1 hr)	% Photo degradation efficiency (For 1 hr)
11.18	3.92	0.70	30
11.66	3.83	0.72	28
14.86	3.62	0.76	24
19.44	3.60	0.79	21
21.28	3.51	0.86	14

*Table 3 :* Lattice parameters and unit cell volume for (101) plane for ZnO nanoparticles at different annealing temperatures

Temperature (°C)	Lattice parameter (a) (Å)	Lattice Parameter (c) (Å)	Unit cell Volume V (Å) <sup>3</sup>
400	3.236	5.177	46.94
450	3.235	5.176	46.91
500	3.233	5.173	46.82
550	3.225	5.160	46.48
600	3.222	5.155	46.35

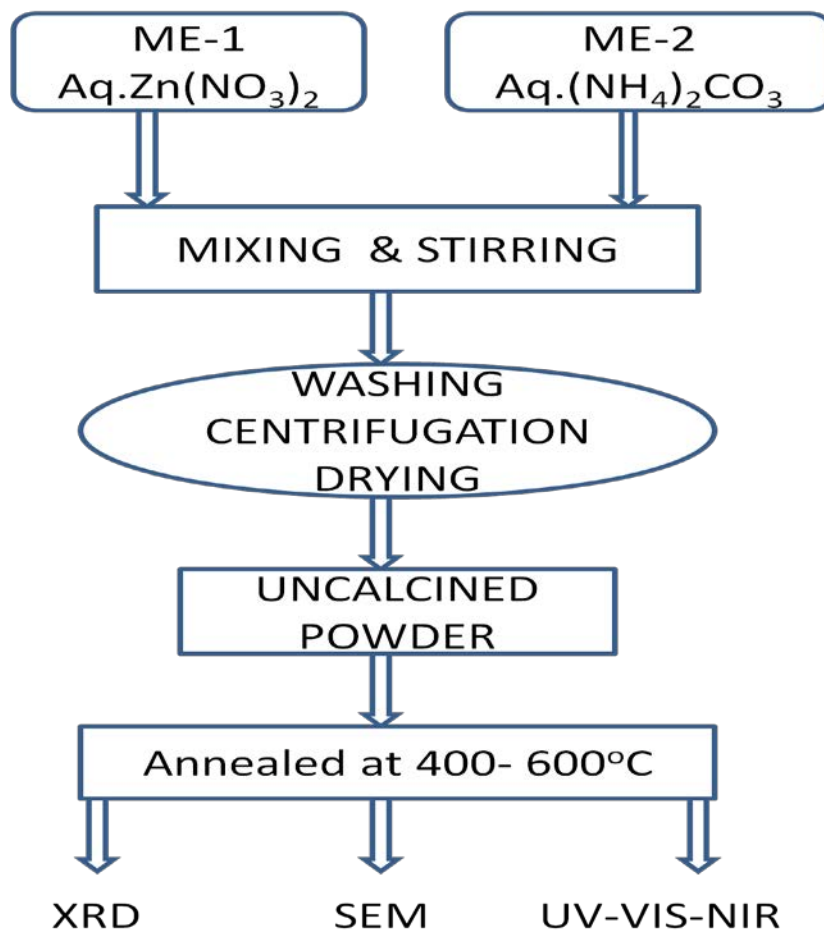


Figure 1 : Flow chart for the synthesis of ZnO nanoparticles by microemulsion method

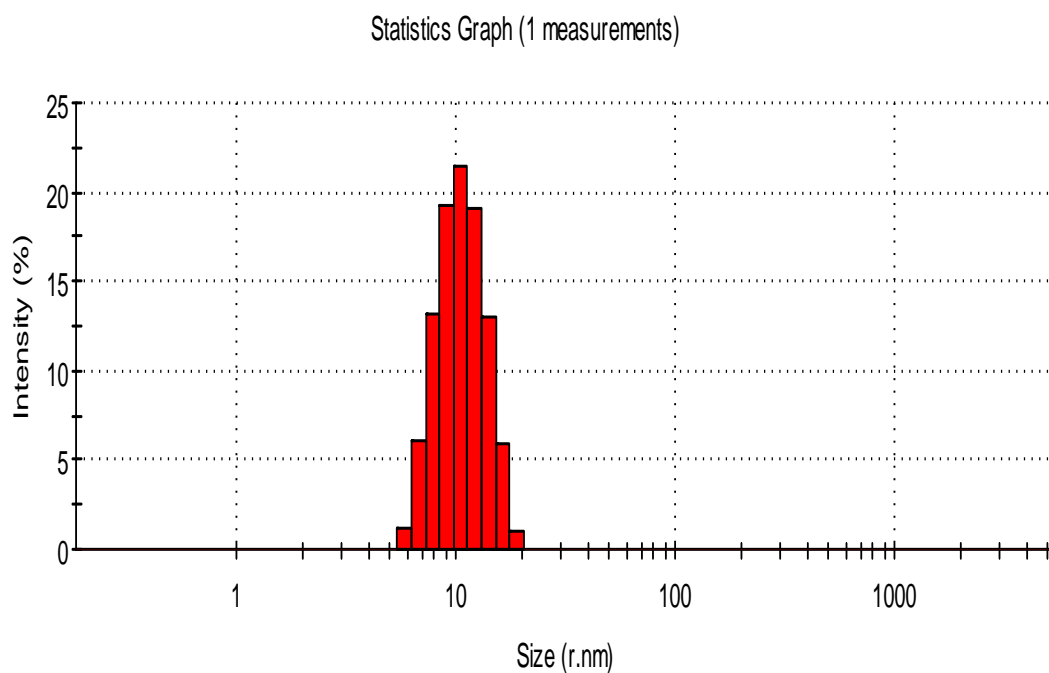


Figure 2 : Core size of microemulsion-1 using particle size analyser

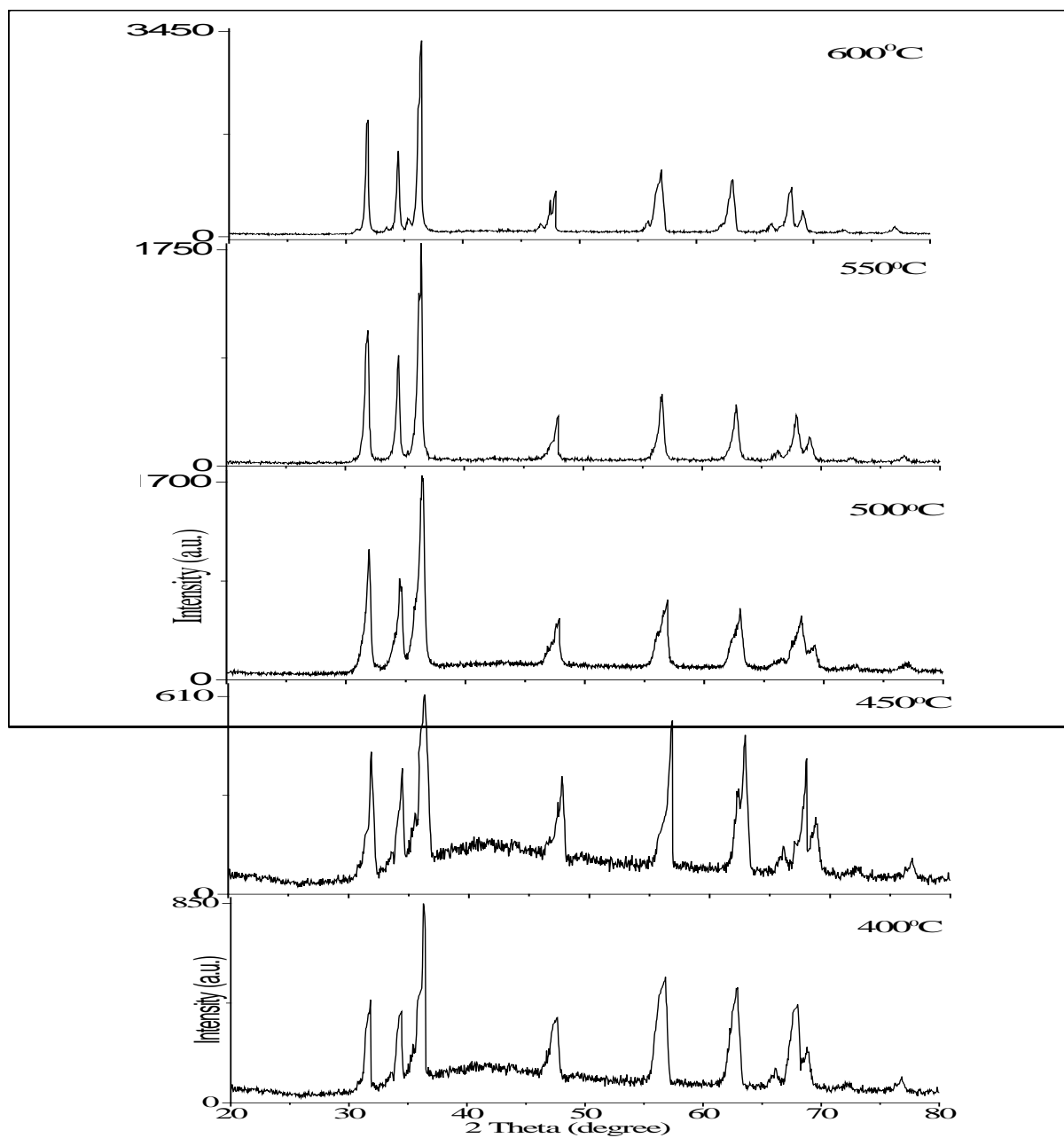


Figure 3 : XRD patterns of ZnO nanoparticles annealed at: (a) 400°C,(b) 450°C,(c) 500°C,(d) 550°C and (e) 600°C

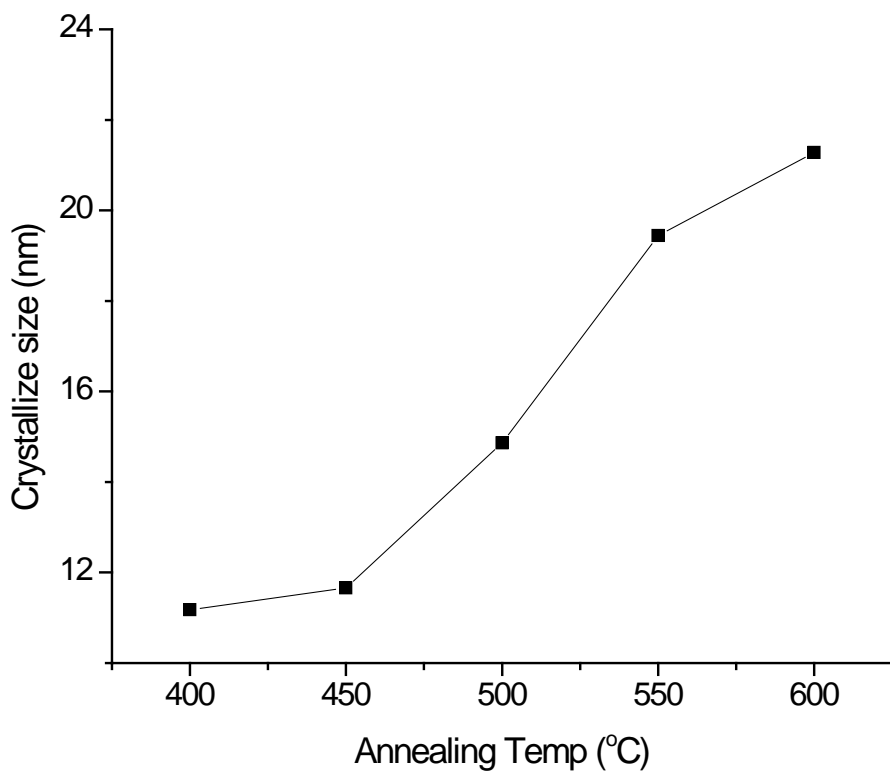


Figure 4 : Crystallite size vs Annealing temperature of ZnO nanoparticles

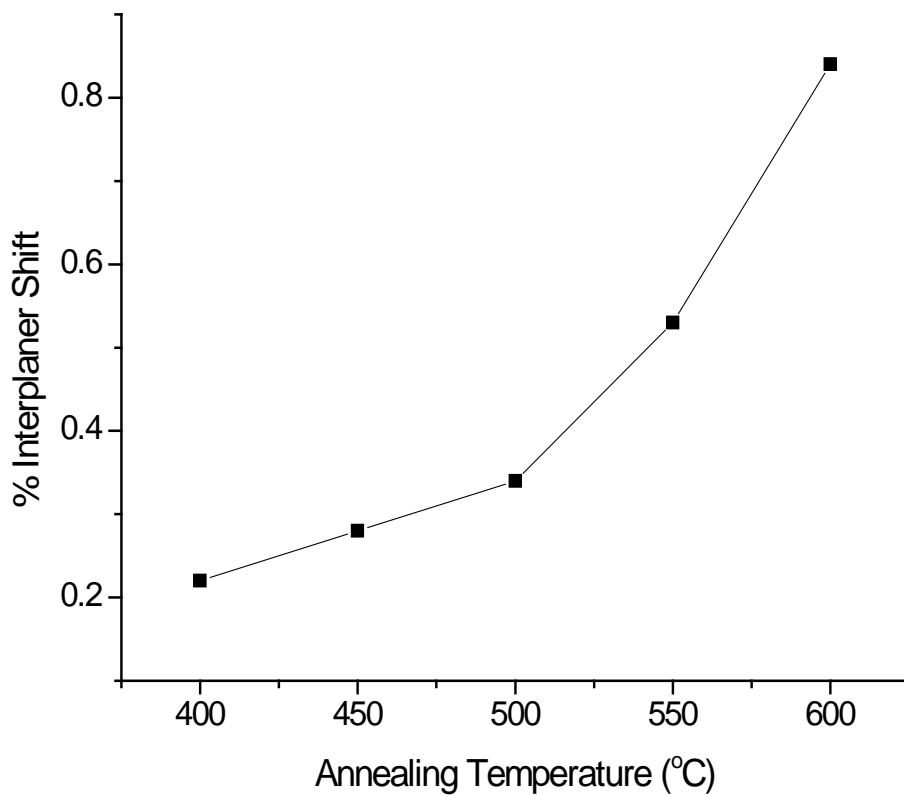


Figure 5 : % Interplaner shift of ZnO NPs at different Annealing temperature

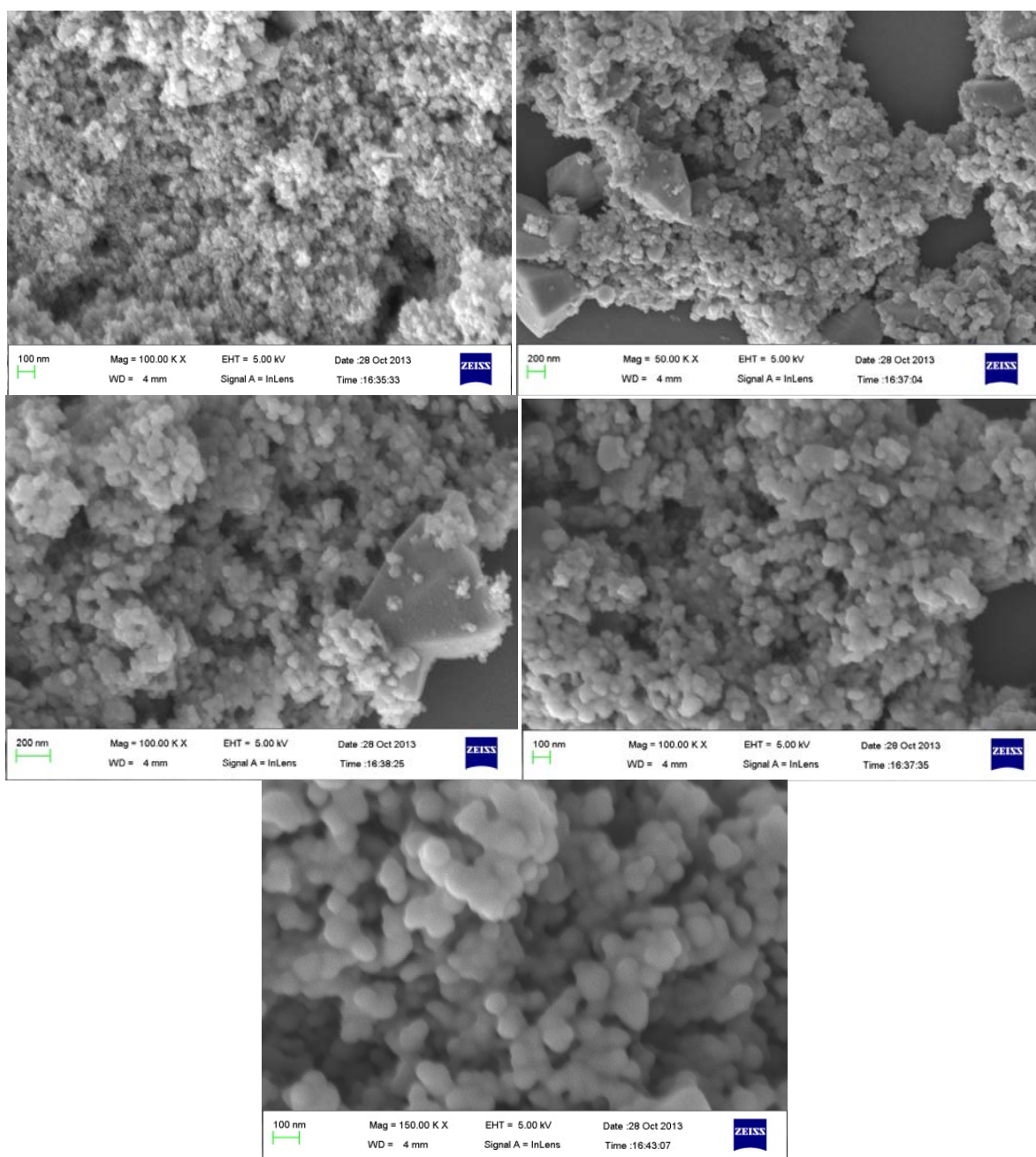


Figure 6 : SEM micrograph of ZnO nanoparticles annealed at (a) 400 (b)450 (c) 500 (d) 550 & (e) 600 °C

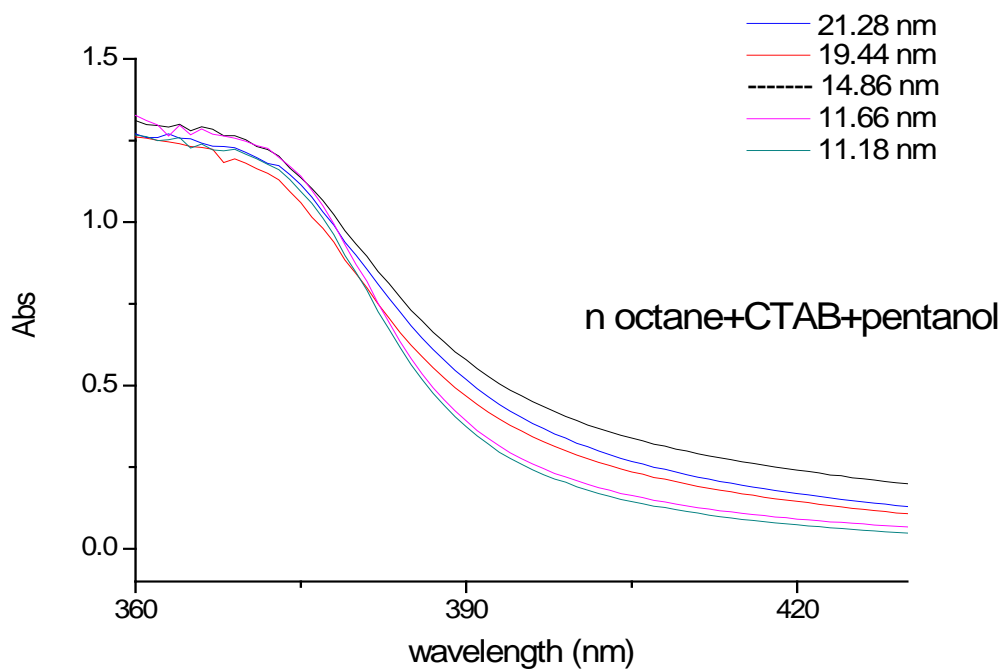


Figure 7 : UV-VIS absorption spectrum of different sized ZnO nanoparticles

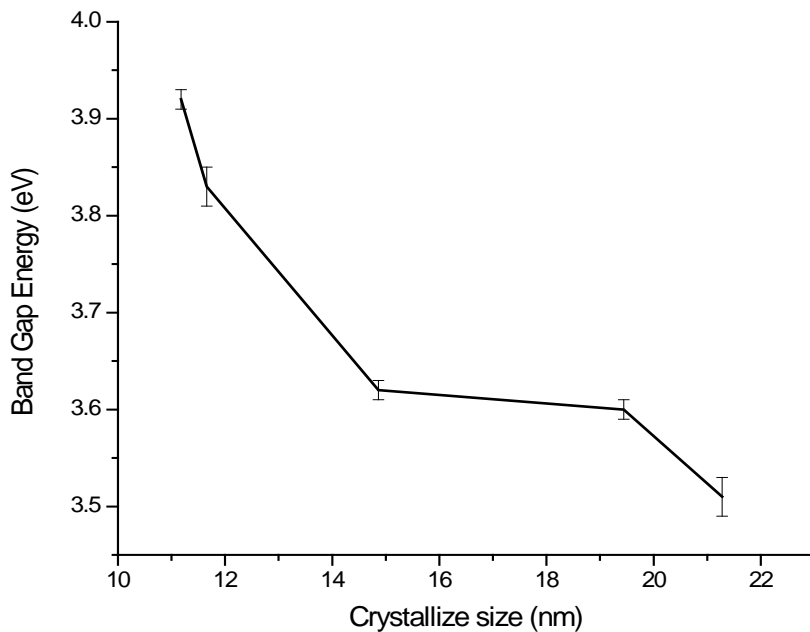


Figure 8 : Crystallite size dependence of band gap energy of ZnO NPs calcined at different temperatures

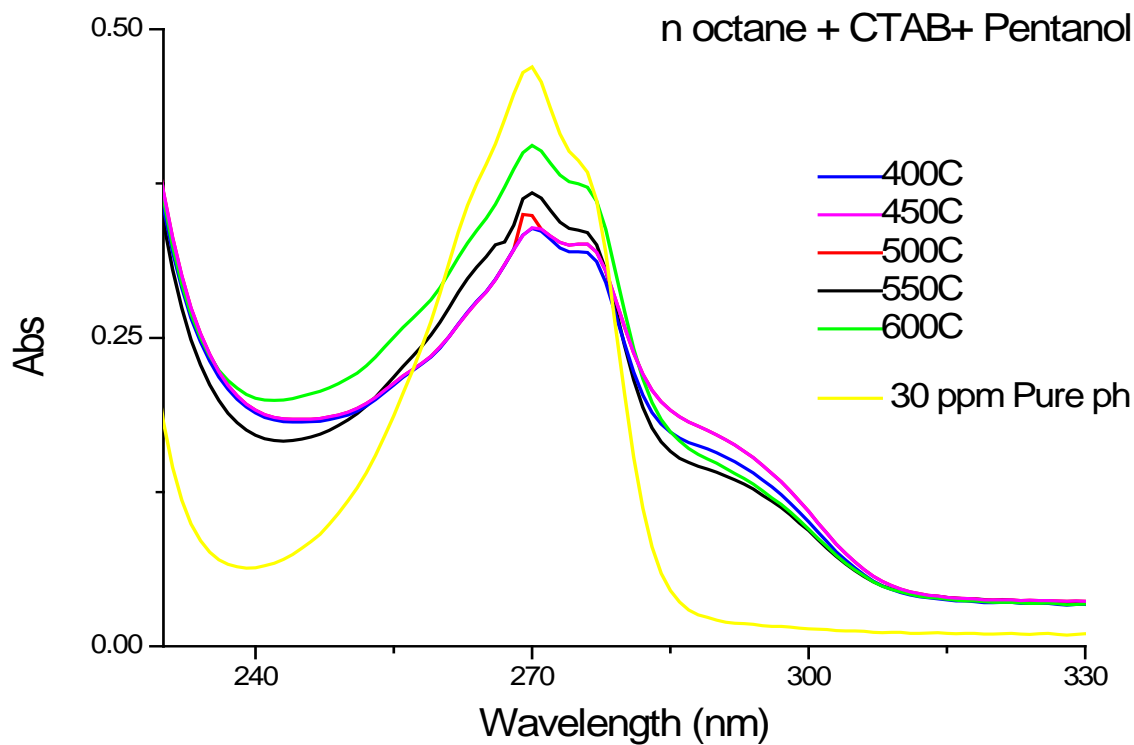


Figure 9 : UV-vis absorption spectra for the degradation of 30 ppm phenol in 1 hour using 1000 ppm ZnO nanoparticles as a catalyst

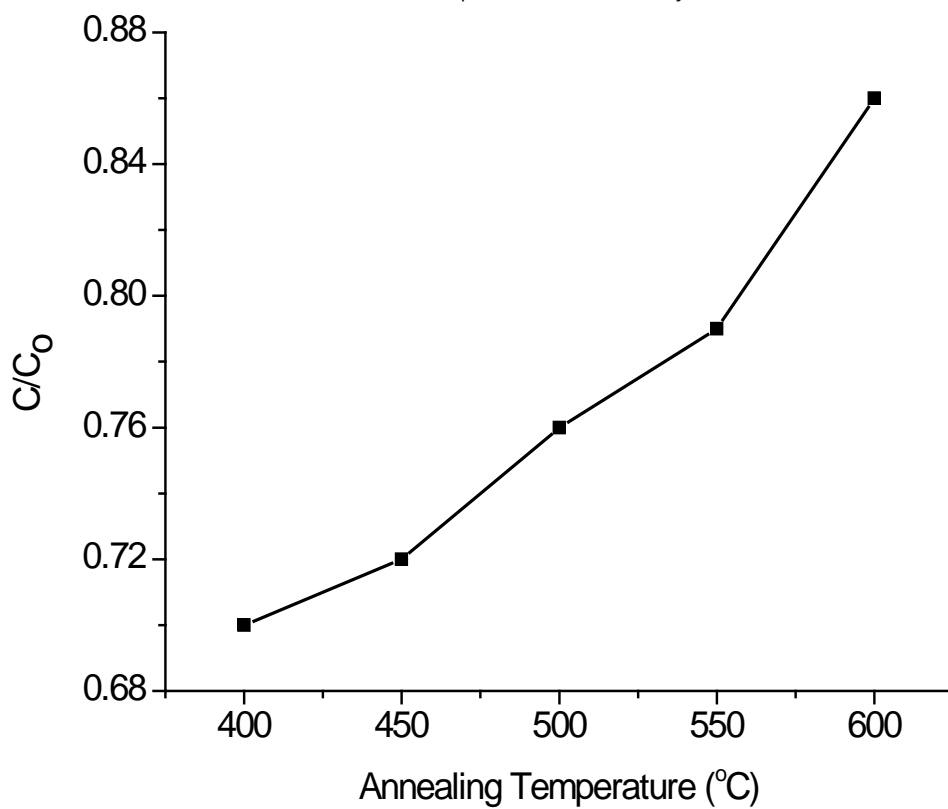


Figure 10 : Plot of  $C/C_0$  vs Annealing temperature of ZnO NPs synthesized by microemulsion

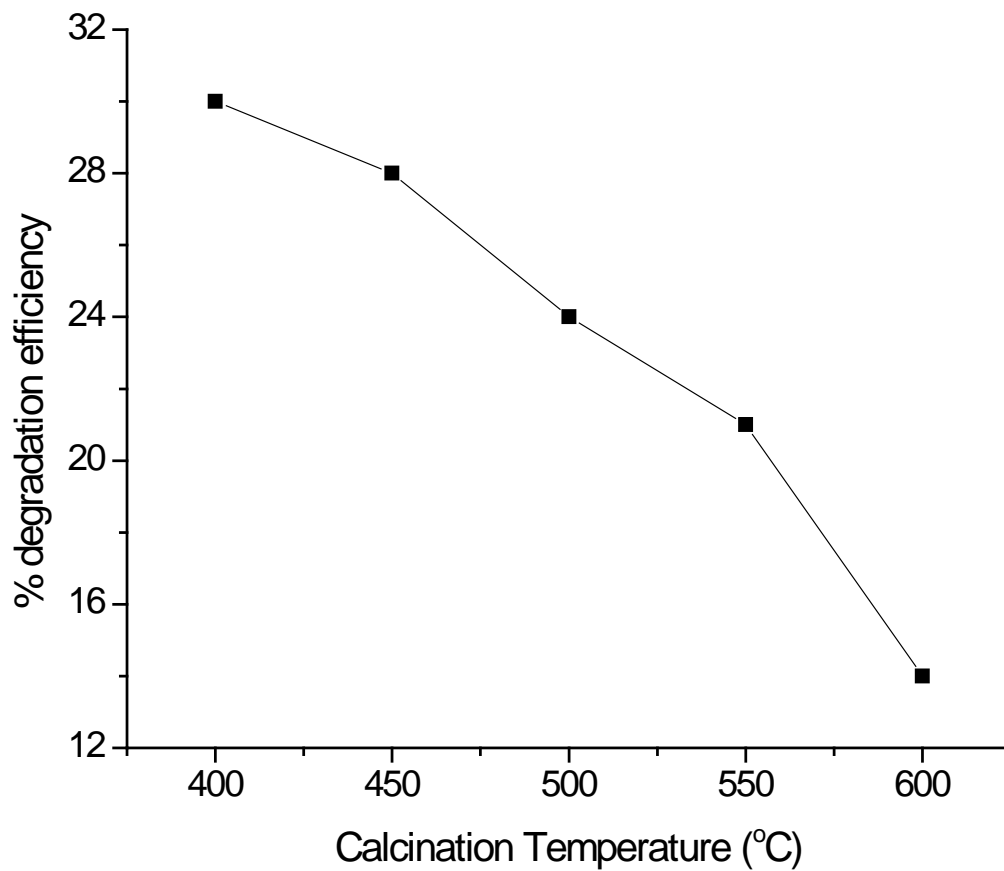


Figure 11 : % degradation efficiency of 30ppm phenol by ZnO NPs annealed at different temperatures

This page is intentionally left blank